Practical Realization of Power and Data Transfer Using WPT Systems

Capstone Report

Anel Murat

Nazarbayev University
Department of Electrical and Computer Engineering
School of Engineering and Digital Sciences

This project report was created on TexStudio editing platform using LaTeX. All the figures were drawn using draw.io online software tool.

Electrical and Computer Engineering
Nazarbayev University
http://www.nu.edu.kz

Title:
Practical Realization of Power and Data Transfer Using WPT Systems

Theme:
Compact Defected Ground Structure-Based Wireless Power and Information Transfer Systems for Biomedical Applications

Project Period:
Spring 2024

Project Group:
High Frequency Measurement and Characterization Laboratory C4.223

Participant(s):
Anel Murat

Supervisor(s):
Mohammad Hashmi

Copies: 1

Page Numbers: 25

Date of Completion:
April 24, 2025

Abstract:

This project presents design of a compact defected ground structure-based wireless power transfer (WPT) systems with dual-band functionality realized for biomedical applications. Design of the first system is specifically optimized to achieve high power transfer efficiency. The development process begins with the design of dual-band resonator with a size of 15-by-15 sq. mm. In particular, design of the resonator optimized to achieve optimal current distribution. Subsequently, WPT is realized by coupling of two designed resonators at a 10 mm transmission range. The power transfer efficiency reaches 79% at 0.9 GHz and 60.5% at 1.8 GHz. Considering the possible misalignment in practical applications, the system's performance was assessed under displacement conditions. According to these results, developed WPT demonstrates stable performance within a specific range of horizontal and vertical shifts.
Based on these results, the second part of the project focuses on realizing a wireless information and power transfer (WIPT) system, followed by an experimental evaluation of its performance in both power and data transfer. Initially, two separate resonators with distinct defects and operating frequencies are designed and then connected in series to form a dual-band resonating structure. The final resonator has a size of 18-by-18 sq. mm and operates at 433 MHz and 900 MHz. Subsequently, two identical resonators are coupled at a 15 mm separation distance to form the WIPT system. The formed WIPT achieves power transfer efficiency of 53.9% at 433 MHz and 54.7% at 900 MHz. In the next step, WIPT's data transmission capabilities are evaluated based on bit-error rate (BER) using a universal software radio peripheral configured through LabVIEW software. Specifically, BER is measured at varying separation distances between the resonators, reaching a minimum value of 0.0318 at 433 MHz and 0.0197 at 900 MHz under perfect alignment. In addition, WIPT is employed for the transmission of text information, which is then analyzed through constellation plots. These plots demonstrate clearly indicated and symmetrically arranged constellation points, indicating accurate transmission.

Contents

Preface **viii**

1 Introduction **1**
1.1 Background Information and Aim 1
1.2 Advancement in WPT systems 3
1.3 Ethical and Professional Responsibilities 5

2 Methodology and Results Discussion **9**
2.1 WPT System Development 10
2.1.1 Design of Dual-Band Resonator 10
2.1.2 WPT System Realization 11
2.1.3 Obtained Results 13
2.2 Development of WIPT System 14
2.2.1 Design of Dual-Band Resonator 14
2.2.2 WIPT System Realization 15
2.2.3 Measurement Results and Discussion 17

3 Conclusion **20**

Bibliography **21**

A Effect of External Capacitors on Operating Frequencies of WPT **24**

Preface

Nazarbayev University, April 24, 2025

Anel Murat
<anel.murat@nu.edu.kz>

Chapter 1

Introduction

1.1 Background Information and Aim

The rapid advancements in new technologies, such as radio-frequency identification [1], electric vehicles [2], unmanned aerial vehicles [3], low-power sensors [4], consumer electronics [5], and biomedical devices [6], have driven a growing interest in innovative powering methods. The vast majority of these applications utilize lithium-ion batteries as the main source of power. Due to limited lifespan, these batteries require to be periodically replaced in cases of depletion, creating a number of complications. Particularly for biomedical devices, such replacements are accomplished by invasive surgeries, which may lead to potential complexities and increased risk of infections [7]. Moreover, integrated batteries contribute to an increase in the overall size of the devices, reducing the comfort for patients [8]. One of the promising solution to the stated problems is integration of Wireless Power Transfer (WPT) systems, enabling the transmission of electrical energy without physical cables.

WPT technologies can be divided into near-field (non-radiative) and far-field (radiative) systems. The latter one is utilized in applications where long range transmission is required, for instance, solar power satellites and drone aircrafts [9]. It is worth noting that this type of WPT systems is not applicable for the biomedical devices due to safety concerns, particularly the risk of tissue damage caused from radiation. In near-field (NF) WPT, electric and magnetic fields are separated, resulting in absence of radiation, and making them safe for utilization in biomedical field. Power transferring in NF WPT systems can be achieved by the following three techniques: capacitive, inductive, and magnetic resonant coupling (MRC). Among these, MRC is the most commonly used method due to its ability to concentrate power at specific frequencies, resulting in more efficient performance [10]. Furthermore, MRC type WPT systems employ three methods for creating the resonators, namely coils, planar structures, and defected ground structure (DGS).

For biomedical applications, a WPT system must achieve both compactness and high efficiency. In addition to these requirements, data transmission capability is another important aspect that should be considered, especially for application in implantable medical devices (IMDs). Thy physiological data collected must be communicated to the controlling device outside the human body for monitoring and detecting abnormalities at early stages [11], [12]. In this regard, the DGS technique provides significant advantages, facilitating the design of compact and efficient WPT systems while supporting multi-band operation for usage in both power and data transfer [2].

IMDs have enabled advanced diagnostics of medical conditions and remote monitoring of vital health parameters, such as cardiac rate, blood pressure, and temperature [13]. With the growing number of patients suffering from chronic diseases like diabetes and cardiovascular disorders, the development of compact, efficient, and multi-band WPT systems has become increasingly important. However, realizing such systems poses challenges related to resonator structure, operating frequency, and overall system efficiency—each of which must be optimized to ensure reliable performance within the constraints of IMDs.

With the aim to fulfill the requirements of compactness and multi-band operation, this project focuses on the realization of a miniature DGS-based WPT systems, having dual-band functionality and suitable for biomedical applications. The design of the first system is optimized to achieve high PTE. Initially, the resonator's area is selected to be 15×15 mm^2 for reaching the highest compactness. For the application in biomedical field, the operating frequencies are selected within the industrial, scientific, and medical (ISM) bands ($902 - 908$ MHz and $2.4 - 2.4835$ GHz) [6]. Subsequently, the WPT system is implemented using the two coupled resonators, functioning at 0.9 GHz and 1.8 GHz. The obtained results show PTE of 79% and 60.50%. Considering the possible practical employment, the system's performance is also evaluated in conditions of horizontal and vertical displacements.

Based on the results of the conducted work, the WIPT system is then developed with subsequent experimental validation of its both power and data transmission capabilities. The first stage of the design process includes the development of the resonator, a fundamental block of the WIPT system. To accomplish this, two separate DGS-based resonators with different defect geometries are developed. These resonators are integrated with external capacitors to achieve resonances at 433 MHz and 900 MHz, respectively. Afterward, the obtained resonating structures are connected in series to a single excitation gap, forming the final resonator with an overall size of 18×18 mm^2. Subsequently, two identical resonators are coupled at an optimal distance of 15 mm to achieve WIPT. The power transfer performance is evaluated in terms of PTE and Figure-of-Merit (FoM) metrics, which are derived from experimental measurements conducted using a vector network analyzer. Specifically, the system achieves 53.9% at 433 MHz and 54.7% at 900 MHz,

which corresponds to FoM values of 0.449 and 0.456, respectively.

As the next step, the WIPT system's performance is assessed in data transmission. Firstly, the selected bit sequence is modulated using a Quadrature Amplitude Modulation (QAM) scheme with a Universal Software Radio Peripheral (USRP). Then, the received data is analyzed for Bit-Error Rate (BER) using the LabVIEW tool, showing the lowest values of 0.0318 and 0.0197 under perfect alignment conditions. Following this, the WIPT system is used to transmit text information. The received signal is analyzed using constellation plots, which indicate accurate symbol detection and minimal distortion.

1.2 Advancement in WPT systems

Extensive research has focused on designing DGS-based WPT systems for different applications. One of the existing single-band WPT systems, proposed in [14], achieves a PTE of 57.9% at 0.403 GHz, with a resonator area equal to 25.5 mm^2. Another example of a WPT system is presented in [15], where two identical resonators of size 31.5×31.5 mm^2 are coupled at a distance of 10 mm. The designed system operates in the 40 MHz frequency band and achieves a PTE of 53.3%.

Apart from single-band WPT, the multi-band WPT systems have attracted considerable attention among the researchers. In addition to power transmission, WPT systems can be designed to facilitate simultaneous power and data transfer, enabling continuous monitoring of a patient's health through biomedical devices, such as cardiac pacemakers [11], brain-machine interfaces [16], and wireless capsule endoscopes [17]. These systems require at least two isolated bands employed one for data and another for power transfer [18].

One commonly employed technique in developing multi-band systems is the cascading method. In this approach, multiple DGS-based resonant circuits or coils are connected in series or parallel, each tuned to a specific frequency. This enables operation over multiple bands, either sequentially or simultaneously. A recent work [19] proposed a dual-band WPT system with two connected in-series semi-H-shaped DGS resonators. By doubling the defect and integrating lumped elements, distinct operating frequencies were achieved. The realized system, with an overall size of 31×13 mm^2, demonstrated PTE of 71% at 433 MHz and 72% at 900 MHz at a separation of 16 mm. While the cascading method provides flexibility and simplicity in resonance control, it also increases the size of the resonator [4].

It is important to note, however, that there are relatively few studies focused on data transmission using WPT systems. One of such study [18] proposed a design of a tri-band WIPT system operating at 300, 433, and 700 MHz, achieving PTE values of 70.1%, 66%, and 65%, respectively. Additionally, the system was tested for up-link and down-link data transfer at 433 and 700 MHz using a universal software radio peripheral (USRP). The results show that a BER of 0 was achieved

at a critical coupling distance of 23 mm, with the BER reaching a maximum of 0.06 as the distance increased to 33 mm. Another study related to data transmission [20] investigated a mixed coupling structure-based WPT system that used dual-frequency coils to improve tolerance to lateral and angular misalignment. The system delivered 0.5 W of power at a 10 mm distance, achieving a PTE of 72.4% and maintaining over 60% PTE under 40 mm lateral or 60° angular misalignment. For data transmission, a 200-kHz frequency-shift keying (FSK)-modulated signal was transmitted directly through the power link, achieving a BER below 10^{-6} and signal noise ratio of 14.19 dB at perfect alignment. In [21], the authors explored bidirectional communication through the power transmission band of a coil-based WPT system. A 30-W prototype operating at 80 kHz was built, with a data transfer rate of 80 Kbps achieved under varying load conditions (10 Ω to 15 Ω). The system demonstrated stable communication even with a 5 mm horizontal misalignment of the coils, without affecting data transmission.

1.3 Ethical and Professional Responsibilities

- **Ethical Responsibility:**
  A number of ethical considerations must be made while designing a WPT system for use in the biomedical field. One of the primary concerns is patient safety. Long-term exposure to electromagnetic (EM) fields can pose health risks due to the heating of biological tissues. To ensure that the system operates within safe power limits, the design approach and choice of substrate were made to comply with the IEEE C95.1-1999 and C95.1-2005 safety guidelines [13]. This is especially important to avoid thermal injury or other adverse biological effects.

  Another concern is the license-free frequency of operation. The system's operating frequencies will be selected within the ISM band, allowing WPT to be utilized without the need for specific licensing. Furthermore, it is essential to note that the degree of energy absorption transmitted by EM fields depends on the frequency of the EM waves. Specifically, lower frequency bands, such as those within the ISM range, have better penetration in human tissues while minimizing excessive heating. Therefore, WPT systems operating within the ISM band are safe to use in the biomedical domain.

  Moreover, in data transfer, the transmission gain is set to 0 dBm in this work to remain within safe power limits.

- **Informed Judgments:**
  The first step in development of WPT system was review of the existing literature on existing single-band and multi-band systems. This allowed to analyze different approaches for the realization of WPT, such as capacitive coupling, inductive coupling, and MRC, used in previous designs and evaluate them in terms of applicability for the development of compact and efficient dual-band system tailored to biomedical applications. Based on this analysis, DGS technique was selected for design of resonators due to its capability to support multi-band operation while enabling miniaturization. Performance characteristics, such as PTE and transmission distance were also analyzed among existing systems for various applications. This allowed to define the parameters of the system and perform optimization with the aim to achieve these requirements. It is important to note that the design and validation process will be conducted initially through simulations utilizing Computer Simulation Technology (CST), followed by experimental evaluations. To assess practical applicability, the system's performance will be assessed under conditions of both horizontal and vertical displacements.

- **Global Context:**
  The number of patients having the chronic diseases and neurodegenerative

disorders increase worldwide. Taking this into account, the dual-band WPT system is highly relevant in terms of global context, especially for managing chronic conditions, such as diabetes, Parkinson's, and Alzheimer's. The implantable medical devices used for management of symptoms rely on lithium-ion batteries, as was mentioned earlier. WPT system presented in this work can potentially increase the lifespan of these devices by reducing the need for periodic invasive battery replacements. This enhancement is especially important, since each replacement surgery possess risks for patient's health, including infections, tissue damage, and discomfort during the recovery process for the patients. In developed countries with advanced healthcare systems, this technology can be relatively easily integrated into the existing medical practices. For example, WPT systems can be integrated into the manufacturing process of IMDs and into the treatment protocols of diseases. However, in developing countries or regions with limited healthcare infrastructure, the scaling and adoption of WPT technology can face significant challenges related to cost of the technology, accessibility, and lack of qualified personnel.

- **Economic Impact:**
  In the short term, the development costs of designing, prototyping, and testing the system could be substantial, especially given the precision required for biomedical applications. However, in the long term, by eliminating the need for battery replacement surgeries, WPT reduces the frequency of invasive procedures, which can be costly and carry associated risks of complications. The system could lower healthcare costs by enabling remote monitoring and reducing the need for invasive procedures. This would make healthcare more efficient and potentially decrease the cost of patient care. Moreover, WPT technology can enhance the lifespan of medical devices by providing a constant power supply, thereby reducing the need for frequent battery replacements that can damage the internal parts of the device. For devices that usually require battery changes every 5 to 10 years, the integration of WPT system can greatly extend their lifespan. This will result in a reduced need for replacements and cost savings for both healthcare providers and patients. However, making this technology affordable for widespread use can be challenging, especially in areas with limited financial resources.

- **Environmental Impact:**
  WPT systems for biomedical applications significantly reduce the environmental impact associated with traditional lithium-ion batteries. Conventional implantable medical devices often rely on these batteries, which have limited lifespans and contribute to substantial electronic waste upon disposal, releasing toxic substances such as heavy metals and solvents into the environment

if not properly managed. By implementing a wireless power transfer system, the need for periodic battery replacements can be eliminated, thereby decreasing the volume of waste generated. This shift not only extends the operational lifetime of implantable devices but also aligns with global sustainability goals by minimizing hazardous electronic waste. The production of these batteries entails substantial extraction of finite resources, including lithium, cobalt, and nickel. Furthermore, the reduction in reliance on non-renewable battery sources directly contributes to resource conservation and diminishes the carbon footprint associated with battery manufacturing and disposal. Moreover, WPT systems provide a constant power supply to medical implants, which helps in maintaining their functionality over longer periods. The implementation of WPT systems can facilitate the design of smaller, more efficient devices that consume less energy, thereby minimizing the resource consumption and environmental impact associated with the manufacturing and disposal of new devices. Overall, the adoption of WPT systems promotes a more sustainable approach in healthcare by reducing battery-related environmental concerns and disposal of medical devices.

- **Societal Impact:**

The development of WPT systems has gained an increasing importance, specifically in the biomedical field due to increasing number of patients with chronic conditions. In this regards, IMDs facilitate the diagnostics and management of chronic diseases by enabling constant monitoring of health parameters. However, IMDs require periodic replacement of the conventional lithium-ion batteries accomplished through surgical interventions, which, besides discomfort, pose risk of inflammations and infections. In this regard, WPT system provide an opportunity to wirelessly recharge the device batteries, eliminating the need for surgeries. Another important aspect related to dual-band functionality of WPT system is ability for both power and data transmission. This implies that data from IMDs can be sent to the external controlling device using WIPT systems. For example, information about heart rate can be continuously transmitted from IMDs to the external device, which allows for timely interventions if abnormal patterns are detected. Additionally, for patients with diabetes, non-invasive blood sugar monitoring can simplify and make the process of constant glucose level monitoring more efficient. Therefore, the capability to support simultaneous power and data transmission can lead to earlier detection and more efficient treatment of diseases at early stages of progression. In design process of WPT systems, quality of life of patients and their comfort are always prioritized. Therefore, the decisions related to the design parameters of the developed WPT

systems focus both on compactness and efficiency, aiming to enhance patient comfort while reducing the size of IMDs. Overall, this work contributes to advancing the functionality of IMDs, enhancing patient care, and improving the long-term management of chronic diseases.

Chapter 2

Methodology and Results Discussion

This work presents the design and realization process of miniaturized and efficient dual-band WPT systems operating within ISM bands. The first part of this section presents a full description of the design and evaluation process of the WPT system specifically optimized for achieving high power transfer efficiency. Based on these results, the next part of the work presents design and assessment of performance of WIPT system with the subsequent assessment of its performance in both power and data transmission in experimental measurements.

In general, the WPT system is realized by magnetic coupling of two resonators, acting as transmitter and receiver, in a face-to-face configuration. In this regard, the resonators characteristics determine the performance of WPT. Therefore, the initial step in WPT design process is development of resonating structure operating at chosen frequencies within the ISM band for both systems present. Subsequently, the WPT and WIPT are achieved by coupling two identical resonators separated by a specific distance. It is worth mentioning that the design and validation procedures are performed using Computer Simulation Technology (CST). The experimental evaluation of power transfer capabilities is conducted using a vector network analyzer in terms of PTE and Figure-of-Merit. Following this, the data transfer performance of the WIPT is assessed through the transmission of predefined bit patterns using a quadrature amplitude modualtion (QAM) scheme implemented with the Universal Software Radio Peripheral (USRP). The received data is then analyzed in terms of bit-error-rate (BER) using the LabVIEW tool. In addition, the WIPT system is tested for transmission of text information which is modulated using Quadrature Phase Shift Keying (QPSK) scheme. The received signal is analyzed using constellation diagrams.

2.1 WPT System Development

2.1.1 Design of Dual-Band Resonator

(a) Resonator design steps.

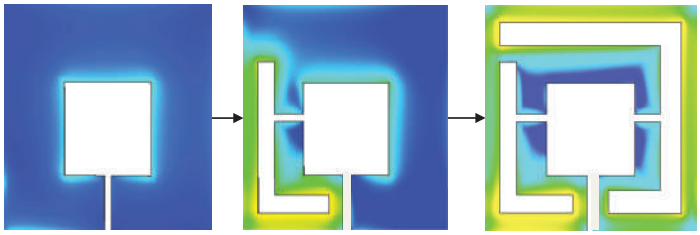

(b) Surface current distribution.

Figure 2.1: Design process and related current distribution.

The principle of the DGS technique, as mentioned earlier, is based on creating a disturbance of current distribution in the circuit by etching a defect on the ground plane. The size and geometry of the defect have significant effect on overall performance of the resonator. Moreover, the optimal current distribution is essential since its ensures maximum power delivery [22].

Keeping the aforementioned in mind, the surface current distribution is evaluated in each design step. Figure 2.1 demonstrates the development steps of the DGS-based resonator and the corresponding surface current distribution. As it can be observed, the insertion of square-shaped defect results in poor surface current distribution, which is then improved by addition of L-shaped defect at the second stage of the design development. In the third stage, incorporation of C-shaped defect leads to the optimal surface current distribution. Therefore, the last design variant is selected for further utilization and optimization.

Fig. 2.2 illustrates the final geometry of the resonator with chosen dimensions of 15×15 mm^2 to ensure its compactness. The resonating structure consists of two copper layers, primarily top- and bottom- sides with thickness of 0.035 mm, separated by a 1.52 mm Rogers' RO4350 substrate ($\epsilon_r = 3.66$). The bottom layer is a ground with etched defect and excitation gap (Eg). The top layer consists of microstrip line (ML) with width (w) and length (l) of 3.4 mm and 15 mm, respectively. The following are the final design parameters of the resonator determined by the

analysis and optimization of surface current distribution: $a = 6.2$ mm, $b = 1.2$ mm, $c = 1.5$ mm, $d = 10$ mm, $x = 12.8mm$, y, and $z = 0.5$ mm. The Eg has dimensions of 0.5×3.7 mm^2.

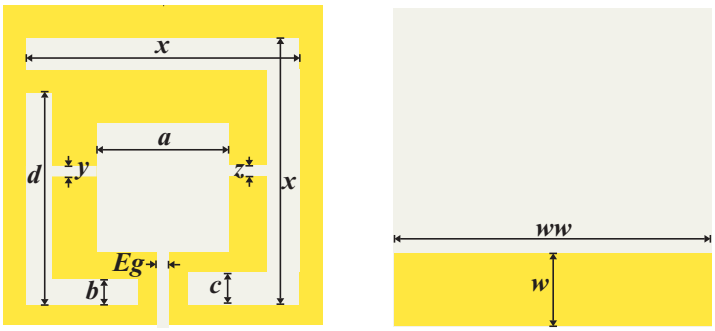

(a) Bottom side. **(b)** Top side.

Figure 2.2: The geometry of the proposed resonator.

The insertion of defect changes the effective capacitance (C) and inductance (L) of ML, resulting in a quasi-lumped resonant circuit behavior with band-stop frequency response [2]. Therefore, the DGS-based resonator can be characterized by its equivalent circuit, which is parallel LC circuit. Here, L and C values depend on the defect shape and Eg, accordingly. Therefore, the resonant frequency can be controlled by changing the defect parameters. The shift in the stop band can be achieved by incorporation of lumped capacitors [23]. The values of L, C, and external capacitors can be determined applying Eq. (2.1) [12].

$$C = \frac{f_c}{4\pi Z_0 \left(f_r^2 - f_c^2\right)}, \quad \text{and} \quad L = \frac{1}{4\pi^2 f_r^2 C}. \tag{2.1}$$

Here, Z_0 is 50Ω, and f_c and f_r represent the -3 dB cut-off and resonant frequencies, respectively. The values of f_c and f_r were determined from S-parameters obtained by electromagnetic simulation performed in CST Studio. In this regard, the lumped capacitors of 0.3 pF and 1.1 pF are inserted into the gaps denoted as y and z to achieve two resonances at 0.9 GHz and 1.8 GHz. Fig. 2.3 demonstrates the obtained results with the operation at the desired frequencies.

2.1.2 WPT System Realization

The operation of WPT system is based on coupling two resonators with their bottom sides facing each other [19]. The transmission range should be properly chosen to prevent over- or under-coupling [2]. It has been determined that the optimal distance between resonators is 10 mm. In addition, to achieve proper Tx and Rx operation at the desired frequencies, external capacitors were integrated into the resonating structures. Their values were determined using iterative method by

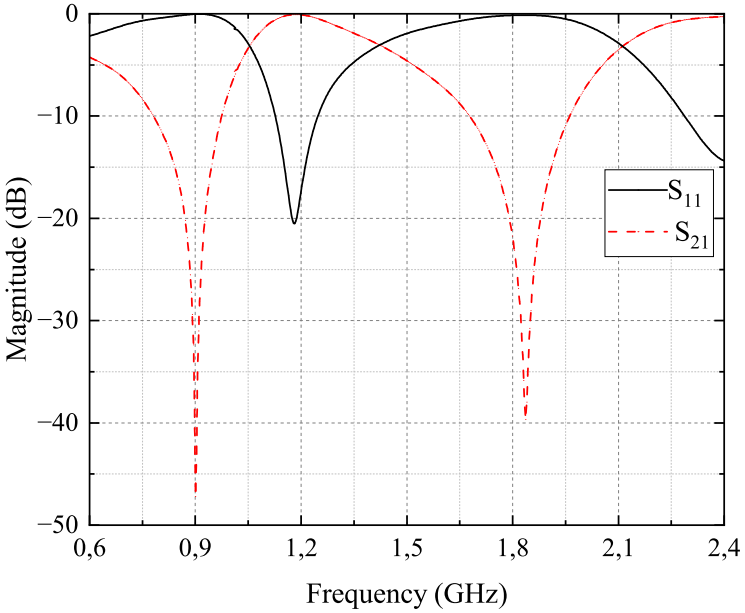

Figure 2.3: Obtained results of developed resonator.

observing frequency shifts as the capacitance varied. Figs. A.1–A.3 show the frequency response of WPT system with different external capacitors incorporated. As it can be observed, increasing capacitance shifts the resonant frequencies to lower bands. The lumped capacitor values required to achieve the interested frequencies were determined to be 0.2 pF and 0.7 pF. Another important factor to consider is impedance matching, achieving which ensures maximum power transfer. When incorporating two coupled resonators, ML functions as an open-circuit terminated stub for impedance matching. The ML length (l_{st}) is determined employing Eq. (2.2) [1]. Here, C_{st} denotes the capacitance of ML necessary to achieve matching at 50 Ω.

$$C_{st} = \frac{1}{2\pi f_r Z_0} \tan(\beta l_{st}), \tag{2.2}$$

Here, β denotes the propagation constant, which is defined as $\beta_n = \frac{2\pi f_r \sqrt{\varepsilon_r}}{c}$. f_r must be specified in MHz [24]. The microstrip line (ML) parameters are further refined based on simulation results to achieve maximum PTE. The optimal value of l_{st} is found to be 11.3 mm.

Finally, the two modified resonators are separated by a distance of 10 mm. The realized WPT system performance characteristics are evaluated in terms of PTE and Figure-of-Merit (FoM), applying Eqs. (2.3) and (2.4) [2, 5].

$$\text{PTE} = \frac{|S_{21}|^2}{1 - |S_{11}|^2} \times 100, \tag{2.3}$$

$$\text{FoM} = \text{Distance} \cdot \frac{\text{PTE}}{\sqrt{\text{Resonator Area}}} \tag{2.4}$$

2.1.3 Obtained Results

Fig. 2.4 demonstrates the simulation results of the developed WPT system. The S_{11} parameter for both frequencies achieves values less than -10 dB, showing a perfect impedance matching. Particularly, for 0.9 GHz and 1.8 GHz S_{11} reaches -19.9 dB and -11.19 dB, accordingly. In turn, S_{21} parameters of -0.664 dB and -2.056 dB correspond to PTE of 79% and 60.5%. Furthermore, the calculated FoM achieves the highest values of 0.527 and 0.403 at a 10 mm transfer range.

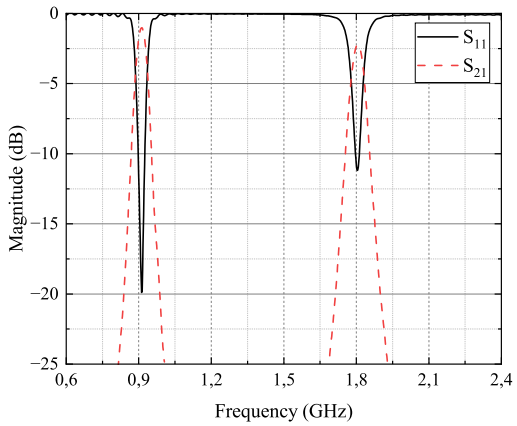

Figure 2.4: Performance results of developed WPT.

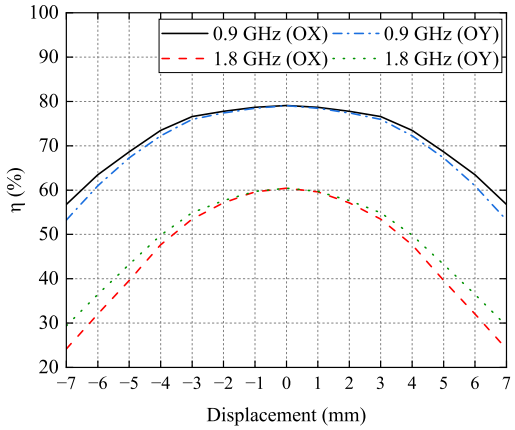

Figure 2.5: PTE vs misalignment.

Besides, since the implemented system is tailored for usage in the biomedical area, there is a high possibility of misalignment occurrence between Tx and Rx in practical scenarios. Thus, it is crucial to evaluate the system's performance under the displacement condition. The misalignment influence on the performance of the designed WPT, specifically PTE, is depicted in Fig. 2.5. It is pertinent to highlight that for this case, the horizontal (OX) and vertical (OY) displacements are considered within the range of ± 7 mm. Based on the obtained outcomes, PTE remains stable under both OX and OY misalignment within ± 3 mm shift at a frequency of 0.9 GHz. When the displacement exceeds this value, PTE slowly decreases, showing significant degradation due to OY than OX displacement. As a result, the greatest reduction of PTE equals 22% at 7 mm misalignment. Meanwhile, a similar reduction in performance can be detected, when OX and OY shifts do not exceed ± 2 mm at 1.8 GHz. For the second frequency, the impact of OX misalignment is greater than OY since the lowest PTE value of 24% is obtained at an OX shift of 7 mm.

Based on the results obtained, the designed system shows only a minimal decrease in PTE at a ± 3 mm shift, indicating stable performance under misalignment. Furthermore, the implemented WPT system shows potential for usage in biomedical applications, given the initial requirements for compactness and multi-band operation.

2.2 Development of WIPT System

In a dual-band system, one band can be used for WPT, while the other can be allocated for WIT [12]. In this configuration, dual-band WPT forms a WIPT system. Therefore, the design process of the WIPT system is similar to that of dual-band WPT. As it was described earlier, the resonator is the fundamental component of the WIPT system, therefore the first stage in the design process is aimed at the realization of DGS-based resonating structure operating at two frequency bands.

2.2.1 Design of Dual-Band Resonator

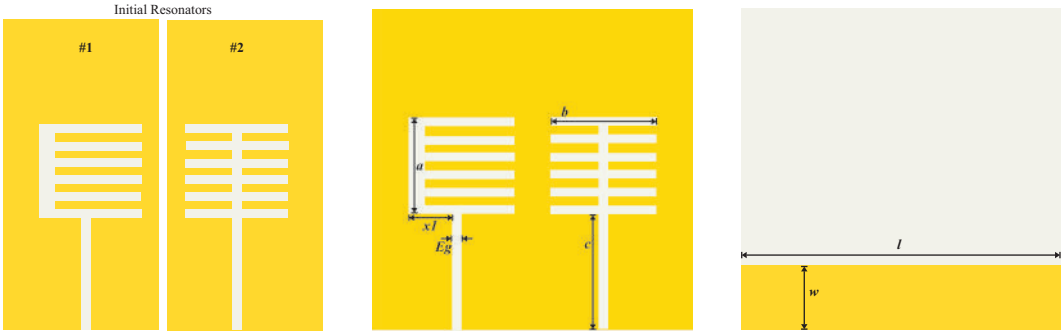

Figure 2.6: The geometry of dual-band DGS resonator.

To achieve dual-band operation, two separate single-band resonators with distinct frequency bands and defect geometries were connected to a single excitation source. Specifically, the operating frequency of the first resonator is set to 433 MHz, while the second resonator is designed to operate at 900 MHz. To meet the requirement for compactness, the overall area of the final resonator is chosen to be 18×18 mm^2, which limits the size of each resonator to 18×9 mm^2, as demonstrated by Fig. 2.6.

In the DGS technique, the resonant frequency is determined by the capacitance and inductance that come from the small excitation gap (C_g) and the metallic part of the ground plane, respectively. Therefore, the resonant frequency (f_r) is defined by the LC combination. In this regard, the values of L and C can be defined by Eq. (2.1), as described earlier in the WPT design procedure.

Initially, f_r of the resonator #1 was equal to 3.36 GHz, which corresponded to L_1 = 4.63 nH and C_{g1} = 0.48 pF. In order to shift the frequency to the desired 433 MHz, an external capacitor (C_{e1}) with value of 12.3 pF was incorporated into the excitation gap of the first resonator, resulting in a total capacitance determined by $C_t = C_e + C_g$.

The same procedure was repeated for adjusting the operating frequency of resonator #2. The initial resonant frequency of 3.52 GHz, corresponding to L_2 = 4.69 nH and C_{g2} = 0.43 pF, was lowered by adding C_{e2} = **[value]** pF to achieve resonance at 900 MHz.

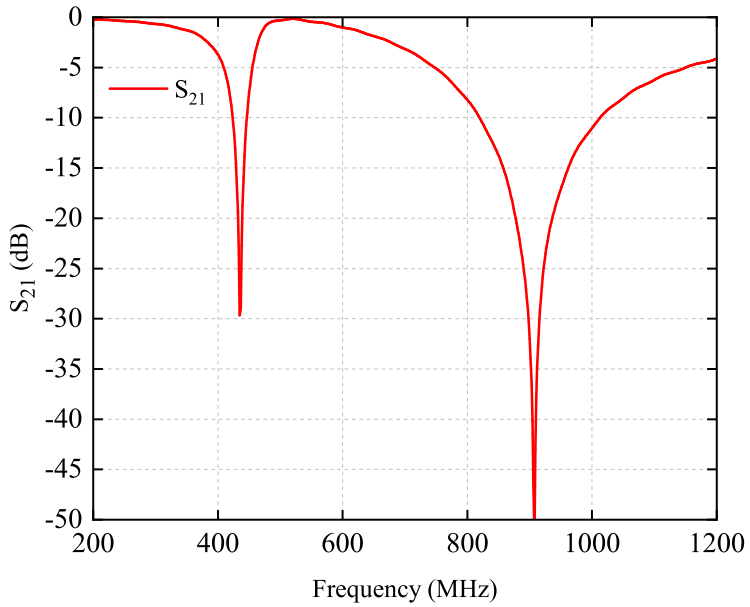

Figure 2.7: Simulation results of dual-band resonator.

The final resonator is realized on a Rogers RT5880B substrate with a thickness of 0.79 mm and copper layer thickness of 0.0175 mm, as demonstrated in Fig. 2.1. The top layer consists of the ML with width denoted by w = 3.4 mm and length l = 18 mm. The characteristic impedance of the ML is modeled to be equal to 50 Ω. The lumped capacitors were adjusted to meet the design requirements of the WIPT system, resulting in final capacitance values of C_{g1} = 12.4 pF and C_{g2} = 3 pF. From Fig. 2.7, two distinct resonance frequencies were observed at the required 433 MHz and 900 MHz, confirming the dual-band operation. The final resonator design parameters are as follows: a = 5.5 mm, b = 6.0 mm, c = 6.5 mm, and $x1$ = 2.5 mm. Meanwhile, the Eg has 0.5 × 3.7 mm^2 dimensions.

2.2.2 WIPT System Realization

The WIPT system is realized by coupling of the two identical resonators with the presented design parameters at an optimal distance which should be accurately

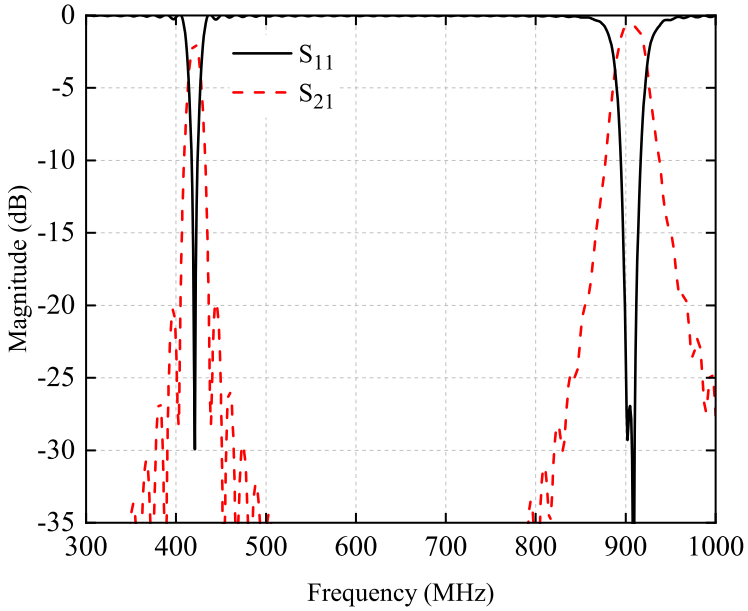

Figure 2.8: Simulation results of the realized WIPT.

defined to avoid undercoupling or overcoupling conditions. To ensure efficient power transfer and minimize reflection losses, the resonators are further optimized for perfect coupling and impedance matching.

Initially, the resonators are brought into proximity to establish the coupling condition. The mutual inductance L_m between the transmitter and receiver is calculated using Eq. (2.5), with $\mathrm{Im}(Z_{21})$ obtained through EM simulation. For this, the ML is removed from the top layer to isolate the response of DGS, lumped ports are introduced at the excitation gaps, and the TX and RX resonators are positioned in a back-to-back configuration.

$$L_m = \frac{\mathrm{Im}(Z_{21})}{2\pi f} \tag{2.5}$$

Then, the impedance matching is achieved by adjusting the ML, which acts as an open-ended stub since the feed ports are connected only to one side of the transmitter and receiver. This stub behaves like a capacitor, and its length is defined using Eq. (2.2), where β is the propagation constant and l_{st} is the length of the stub. After the optimization of the parameters, the values of C_{g1} and C_{g2} was adjusted to 12.4 pF and 2.4 pF, respectively. The optimal length of MLs were found to be 13.25 mm and 5 mm. In order to accommodate them, the location of the excitation gaps was changed, as can be observed in Fig.

The EM results are presented in Fig. 2.8, which show that system operates at the desired 433 MHz and 900 MHz with S_{11} reaching values lower than -10 dB at both bands.

2.2.3 Measurement Results and Discussion

In order to validate the simulation results, the system was further fabricated for the experimental measurements. Beyond power transfer efficiency evaluation, WIPT was also assessed in terms of its data transmission capabilities in both bands. The subsections below provide the detailed descriptions of the steps followed in the experimental evaluation of the system's performance in both power and information transfer.

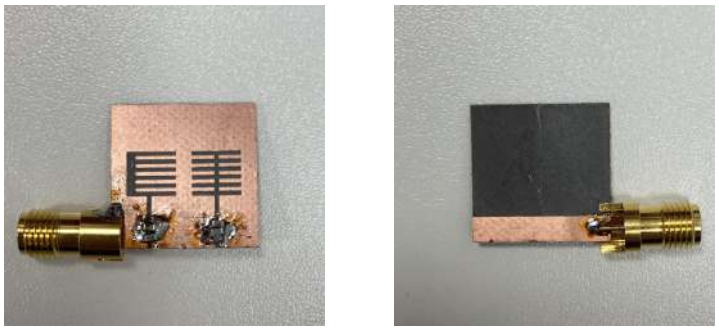

(a) Bottom side. **(b)** Top side.

Figure 2.9: Fabricated prototype of the proposed DGS-based resonator.

Measurement of WIPT System's Power Transfer Capabilities

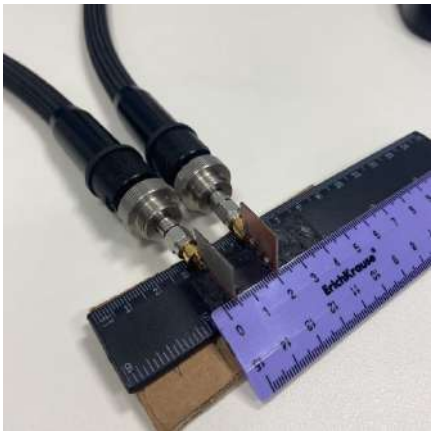

Figure 2.10: The measurement setup.

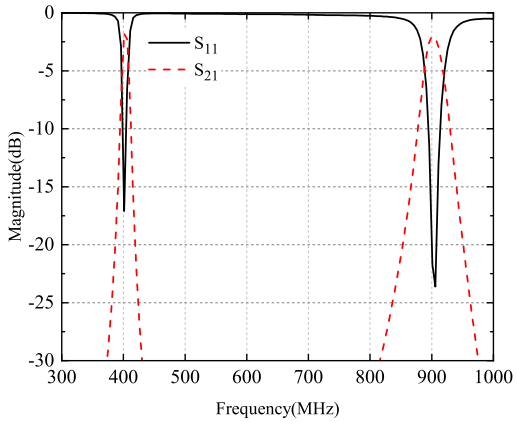

Figure 2.11: Experimental results of designed WIPT.

The characterization of the system's performance in power transfer was carried out by defining its PTE and FoM at both frequencies. Firstly, two resonators with the proposed design were fabricated using the same material as in the simulations, as demonstrated by Fig. 2.9. Then, SMD-type capacitors were soldered onto both

resonators. Subsequently, the obtained Tx and Rx were separated by a distance of 15 mm and connected to the Keysight Vector Network Analyzer (PNA-X, N5247B) through SMA connectors, as depicted in Fig. 2.10.

Fig. 2.11 demonstrates the resonance characteristics obtained, according to which S_{21} reaches values of -2.77 dB and -2.64 dB at 401 MHz and 904 MHz, respectively. Additionally, both bands exhibit S_{11} values of less than -10 dB, specifically -17.09 at 401 MHz and -23.61 at 904 MHz, indicating excellent impedance matching. Furthermore, the respective magnitudes of the measured S-parameters can be substituted into Eqs. (2.3)–(2.4) to assess the PTE and FoM. At the 401 MHz band, these results correspond to PTE and FoM of 53.9% and 0.449, respectively. For the 904 MHz band, the PTE reached 54.7%, corresponding to FoM of 0.456.

Assessment of WIPT system's performance in data transmission

Data transmission is performed using two NI USRPs-2932, acting as Tx and Rx, each connected to its respective resonator via SMA cables. The USRPs are configured through National Instruments LabVIEW graphical interface. Specifically, in the setup, the Tx-USRP generates a data stream modulated with a QAM scheme, serving as the input to the transmitting resonator. The Rx-USRP analyzes the data received from the Rx resonator to assess the performance. Specifically, two cases are considered. In the first case, predefined bit sequence is transmitted and then analyzed through BER metrics at varying transmission distances for 433 MHz and 900 MHz. In the second case, the text information is sent and then analyzed in terms of constellation diagrams.

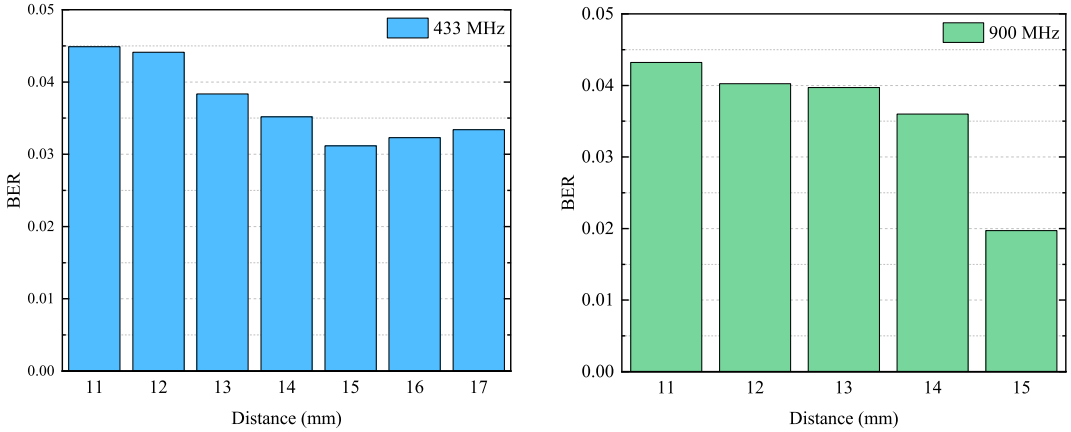

(a) 433 MHz **(b)** 900 MHz

Figure 2.12: BER vs. distance for the developed DGS-based WIPT system.

Fig. 2.12 demonstrates the results obtained. Here, the minimum BER of 0.0318 and 0.0197 were observed at a separation distance of 15 mm for both 433 MHz and 900 MHz, respectively, which indicates that this transmission range corresponds to

the critical coupling condition for the WIPT [18]. In this case, external coupling is matched to the internal losses of the system, which reduces signal reflection [25]. This, in turn, improves the signal quality received at Rx side, corresponding to the lowest BER achieved. Moreover, as it can be observed from Fig.2.12a, deviation in either direction from this optimal distance lead to increase in BER. Thus, the highest BER was found at 11 mm, specifically 0.0449 for 433 MHz and 0.0432 for 900 MHz, which represents the greatest deviation from 15 mm and corresponds to the highest level of under-coupling, while at a perfect alignment the system demonstrated the lowest value.

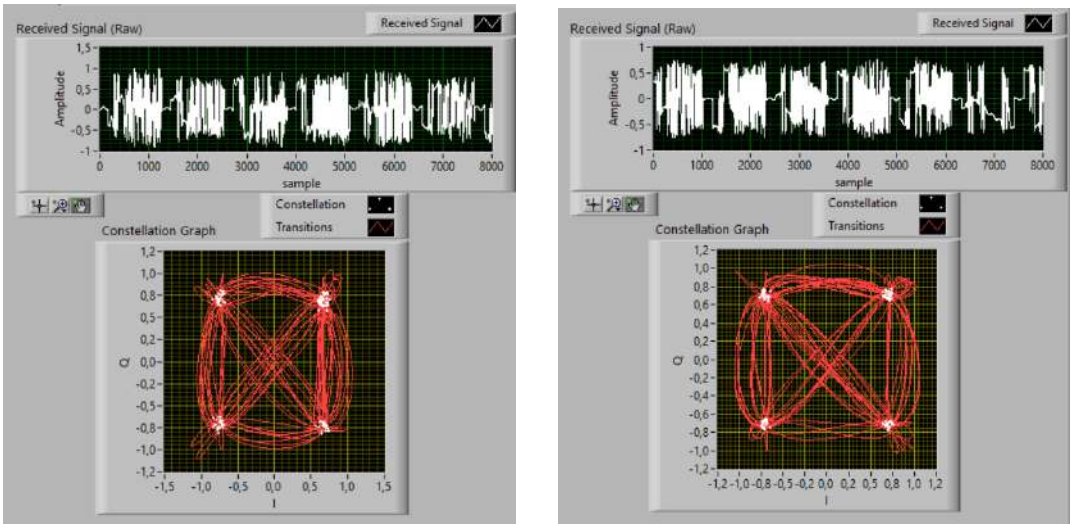

(a) 433 MHz **(b)** 900 MHz

Figure 2.13: Constellation diagram computed at 15 mm distance.

Fig. 2.13 demonstrates the constellation plots obtained during the transmission of text information at perfect coupling condition. The message text was modulated using Quadrature Phase Shift Keying scheme and sent via packet-based transmission. Since the system is tailored for biomedical applications, it is important to consider safety aspects. Specifically, prolonged exposure to time-varying electromagnetic fields can potentially affect human health [27]. To align with the safety guidelines established by the IEEE standard, the transmission gain was therefore limited to 0 dBm (1 mW). As seen in the plots, signals at both frequencies show clear and symmetrical constellation points, indicating accurate symbol detection and minimal distortion.

Chapter 3

Conclusion

This project presents the realization and experimental validation of a WPT and WIPT systems, tailored for biomedical applications. The compactness and efficiency of the WPT and WIPT systems were critical design considerations, especially considering the practical application in low-power biomedical devices. The first step in development process of WPT included the design of resonators applying DGS technique. Obtained resonator had two distinct operating frequencies of 0.9 GHz and 1.8 GHz. The realized WPT system was optimized to achieve high power transfer efficiency, reaching 79% at 0.9 GHz and 60.5% at 1.8 GHz, while demonstrating stable performance under misalignment with minimal drop in efficiency within a range of ± 3 mm horizontal and vertical shifts.

Following the WPT design, the WIPT system was realized by coupling two resonators operating at 433 MHz and 900 MHz. The WIPT system subsequently achieved power transfer efficiencies of 53.9% at 433 MHz and 54.7% at 900 MHz. The data transmission capabilities were evaluated through BER measurements, showing minimum of 0.0318 at 433 MHz and 0.0197 at 900 MHz under perfect alignment. The system's performance was further assessed by transmitting text information. The constellation plots obtained showed accurate transmission and minimal distortion.

These results demonstrate that WIPT systems have significant potential for practical use in biomedical devices, particularly in applications that require both power and information transmission.

Bibliography

[1] F. Ferreira et al. "Compact Near Field Wireless Energy Transfer Systems Using Defected Ground Structures". In: *IEEE J. Microw.* 3.3 (2023), pp. 951–961. DOI: 10.1109/JMW.2023.3257122.

[2] K. Dautov et al. "Quantifying the Impact of Slow Wave Factor on Closed-Loop Defect-Based WPT Systems". In: *IEEE Trans. Instrum. Meas.* 71.Art no. 8004310 (2022), pp. 1–10. DOI: 10.1109/TIM.2022.3181938.

[3] Merey Zhumayeva et al. "Wireless energy and information transfer in WBAN: A comprehensive state-of-the-art review". In: *Alex. Eng. J.* 85 (2023), pp. 261–285. ISSN: 1110-0168. DOI: 10.1016/j.aej.2023.11.030.

[4] K. Dautov et al. "Compact Multifrequency System Design for SWIPT Applications". In: *Int. J. RF Microw. Comput.-Aided Eng.* 31.6 (2021), e22632.

[5] Z. Kudaibergenova and M. Hashmi. "Experimental Performance Evaluation of Compact WPT System for Biomedical Applications". In: (2023), pp. 447–449. DOI: 10.1109/APMC57107.2023.10439875.

[6] S. M. A. Shah et al. "Ultraminiaturized Triband Antenna With Reduced SAR for Skin and Deep Tissue Implants". In: *IEEE Trans. Antennas Propag* 70.9 (2022), pp. 8518–8529. DOI: 10.1109/TAP.2022.3177487.

[7] T. Ninikrishna, P. A., and Z. Mishra. "Optimal Wireless Power Transfer Techniques for Passive Deep Brain Stimulation Devices". In: (2020), pp. 1–5. DOI: 10.1109/INOCON50539.2020.9298441.

[8] A. Basir and H. Yoo. "A Quadband Implantable Antenna System for Simultaneous Wireless Powering and Biotelemetry of Deep-Body Implants". In: (2020), pp. 496–499. DOI: 10.1109/IMS30576.2020.9223826.

[9] H. Atallah, R. Hussein, and A. Abdel-Rahman. "Compact Coupled Resonators for Small Size Dual-Frequency Wireless Power Transfer (DF-WPT) Systems". In: *IET Microw. Antennas Propag.* 14 (Apr. 2020). DOI: 10.1049/iet-map.2018.5693.

[10] K. Dautov et al. “Recent Advancements in Defected Ground Structure-Based Near-Field Wireless Power Transfer Systems”. In: *IEEE Access* 8 (2020), pp. 81298–81309. DOI: 10.1109/ACCESS.2020.2991269.

[11] I. A. Shah et al. “Efficient Wirelessly-Powered Biotelemetric System for IoMT-Enabled Leadless Pacemakers in Dynamic Cardiac Environments”. In: *IEEE Internet Things J.* (2024), pp. 1–1. DOI: 10.1109/JIOT.2024.3491735.

[12] Zhanel Kudaibergenova, Kassen Dautov, and Mohammad Hashmi. “Compact Metamaterial-Integrated Wireless Information and Power Transfer System for Low-Power IoT Sensors”. In: *Alex. Eng. J* 92 (2024), pp. 176–184. ISSN: 1110-0168. DOI: 10.1016/j.aej.2024.02.058.

[13] F. Faisal and H. Yoo. “A Miniaturized Novel-Shape Dual-Band Antenna for Implantable Applications”. In: *IEEE Trans. Antennas Propag* 67.2 (2019), pp. 774–783. DOI: 10.1109/TAP.2018.2880046.

[14] J. Wang et al. “A 403 MHz Wireless Power Transfer System With Tuned Split-Ring Loops for Implantable Medical Devices”. In: *IEEE Trans. Antennas Propag* 70.2 (2022), pp. 1355–1366. DOI: 10.1109/TAP.2021.3111520.

[15] Q. Wang et al. “Wireless Power Transfer System With High Misalignment Tolerance for Bio-Medical Implants”. In: *IEEE Trans. Circuits Syst. II* 67.12 (2020), pp. 3023–3027. DOI: 10.1109/TCSII.2020.2985056.

[16] C. Kim et al. “A 3 mm × 3 mm Fully Integrated Wireless Power Receiver and Neural Interface System-on-Chip”. In: *IEEE Trans. Biomed. Circuits Syst.* 13.6 (2019), pp. 1736–1746. DOI: 10.1109/TBCAS.2019.2943506.

[17] S. Shah et al. “Four-Port Triple-Band Implantable MIMO Antenna for Reliable Data Telemetry in Wireless Capsule Endoscopy and Deep Tissue Applications”. In: *IEEE Trans. Antennas Propag.* 72.8 (2024), pp. 6229–6241. DOI: 10.1109/TAP.2024.3413341.

[18] S. Verma et al. “Measurements and Characterization of a Newly Developed Novel Miniature WIPT System”. In: *IEEE Trans. Instrum. Meas.* 70 (2021), pp. 1–11. DOI: 10.1109/TIM.2021.3075537.

[19] S. Malhotra et al. “Dual-Band WPT System Using Semi-H DGS for Biomedical Applications”. In: (2019), pp. 720–722. DOI: 10.1109/APMC46564.2019.9038176.

[20] T.-C. Yu, W.-H. Huang, and C.-L. Yang. “Design of Dual Frequency Mixed Coupling Coils of Wireless Power and Data Transfer to Enhance Lateral and Angular Misalignment Tolerance”. In: *IEEE J. Electromagn. RF Microw. Med. Biol.* 3.3 (2019), pp. 216–223. DOI: 10.1109/JERM.2019.2898347.

[21] H. Zheng et al. “Data Transmission through Energy Coil of Wireless Power Transfer System”. In: *IEEE PELS Workshop Emerg. Technol.: Wireless Power Transfer*. Chongqing, China, 2017, pp. 1–4. DOI: 10.1109/WoW.2017.7959373.

[22] D. Barth et al. “Resonance Behavior of Low Frequency Metamaterial Cells”. In: (2020), pp. 248–251. DOI: 10.1109/WPTC48563.2020.9295577.

[23] H. A. Atallah, R. Huseein, and A. B. Abdel-Rahman. “Novel and Compact Design of Capacitively Loaded C-shaped DGS Resonators for Dual Band Wireless Power Transfer (DB-WPT) Systems”. In: *AEU Int. J. Electron. Commun.* (2019). DOI: 10.1016/j.aeue.2018.12.016.

[24] K. Dautov et al. “Analysis and Experimental Validation of Circularly Slotted Near-Field WPT Systems”. In: *IEEE Int. Midwest Symp. Circ. Syst.* 2021, pp. 263–266. DOI: 10.1109/MWSCAS47672.2021.9531671.

[25] David M. Pozar. *Microwave Engineering*. 4th. Hoboken, NJ: Wiley, 2012, pp. 439–440.

[26] R. K. Gulati et al. “Characterization of Magnetic Communication Through Human Body”. In: *IEEE 19th Annu. Consumer Commun. Networking Conf.* Las Vegas, NV, USA, 2022, pp. 563–568. DOI: 10.1109/CCNC49033.2022.9700669.

[27] IEEE Standards Association. *IEEE Standard for Safety Levels with Respect to Human Exposure to Electric, Magnetic, and Electromagnetic Fields, 0 Hz to 300 GHz*. IEEE Std C95.1-2019. 2019. DOI: 10.1109/IEEESTD.2019.8859679. URL: https://doi.org/10.1109/ieeestd.2019.8859679.

Appendix A

Effect of External Capacitors on Operating Frequencies of WPT

This section provides frequency response of WPT system with some examples of external capacitors incorporated during the iterative method implementation.

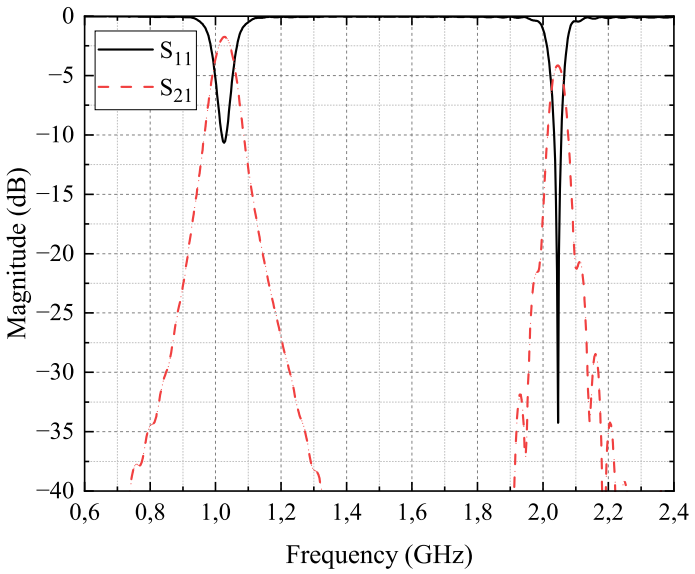

Figure A.1: S-parameter results for 0.12 pF and 0.35 pF.

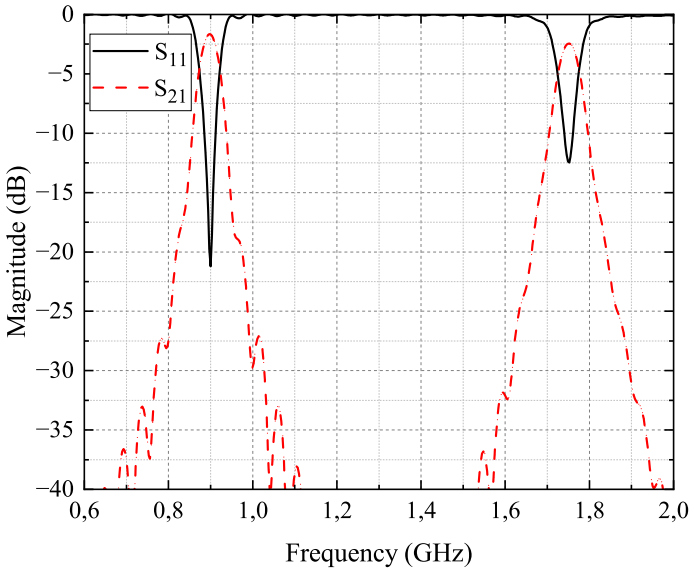

Figure A.2: S-parameter results for 0.25 pF and 0.7 pF.

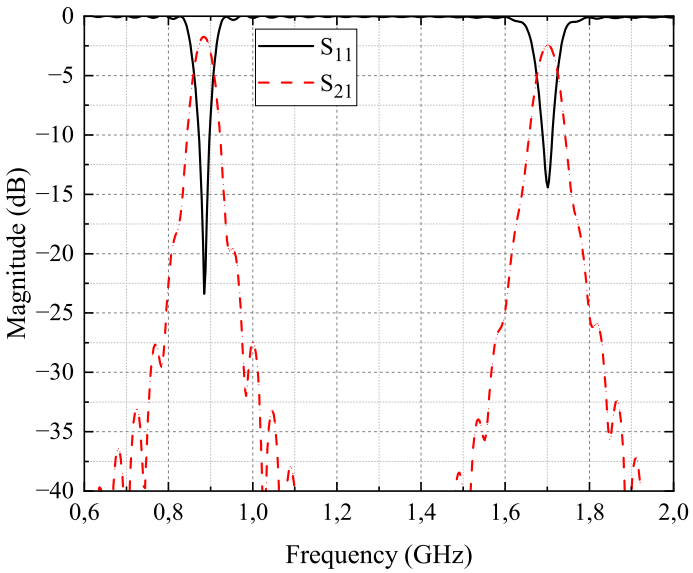

Figure A.3: S-parameter results for 0.3 pF and 0.8 pF.